WILEY-VCH

Supporting Information

Greatly Enhanced Photoluminescence from a Si/WS_2/Si_3N_4/Ag Nanocavity by Exploiting the Electron Transfer Induced by Femtosecond Laser Pulses

Shimei Liu, Zhuo Wang, Shulei Li, Yuheng Mao, Mingcheng Panmai, Jinhao Zhou, Dong Yan, Yongyao Li, Dongxu Zhao, and Sheng Lan**

S. Liu, J. Zhou, D. Yan, Y. Li, D. Zhao
Guangdong-HongKong-Macao Joint Laboratory for Intelligent Micro-Nano Optoelectronic Technology
School of Physics and Optoelectronic Engineering
Foshan University
Foshan 528225, P. R. China
E-mail: zhaodx@fosu.edu.cn
Z. Wang, Y. Mao, S. Lan
Guangdong Provincial Key Laboratory of Nanophotonic Functional Materials and Devices
School of Optoelectronic Science and Engineering
South China Normal University
Guangzhou 510006, P. R. China
E-mail: slan@scnu.edu.cn
S. Li
School of Optoelectronic Engineering
Guangdong Polytechnic Normal University
Guangzhou 510665, P. R. China
M. Panmai
Division of Physics and Applied Physics
School of Physical and Mathematical Sciences
Nanyang Technological University
Singapore 637371, Singapore

Supplementary Note 1

In Figure S1a, we present the scattering spectra calculated for a $Si/Si_3N_4/Ag$ nanocavity and a Si nanoparticle. It can be observed that MD and ED resonances supported by the $Si/Si_3N_4/Ag$ nanocavity exhibit narrower linewidths than those in the Si nanoparticle. Figure S1b shows the calculated scattering spectrum of a nanocavity excited by a plane wave at an incident angle of 53°. In contrast to the normal incidence case (see Figure 5a), the excitation of oblique incidence enables the scattering spectrum of the nanocavity to exhibit a MQ resonance at ~592 nm, which is consistent with the experimental results.

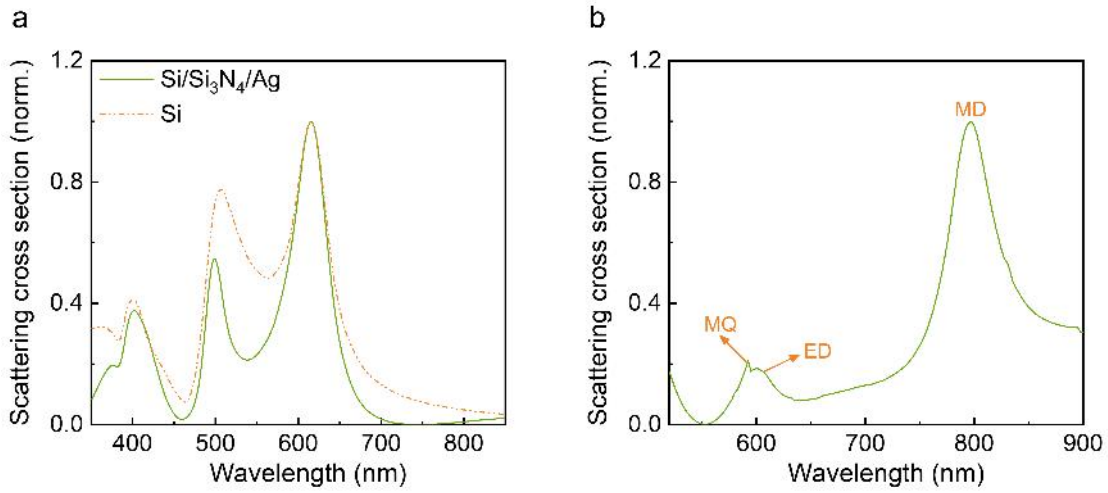

Figure S1. (a) Scattering spectra calculated for a $Si/Si_3N_4/Ag$ nanocavity (d = 150 nm) and a Si nanoparticle (d = 152 nm) on a SiO_2 substrate. (b) Scattering spectrum calculated for a $Si/Si_3N_4/Ag$ nanocavity (d = 203.0 nm) excited by a plane wave at an incident angle of 53°.

Supplementary Note 2

In Figure S2, we present the 1PA spectra calculated for a WS_2 monolayer on a Si_3N_4/Ag heterostructure and a WS_2 monolayer embedded in a Si/Si_3N_4/Ag nanocavity. It can be observed that the 1PA in the embedded WS_2 monolayer is significantly enhanced (shaded region), exhibiting an intensity ~21.4 times higher than that in the WS_2 monolayer on the Si_3N_4/Ag heterostructure (dashed line).

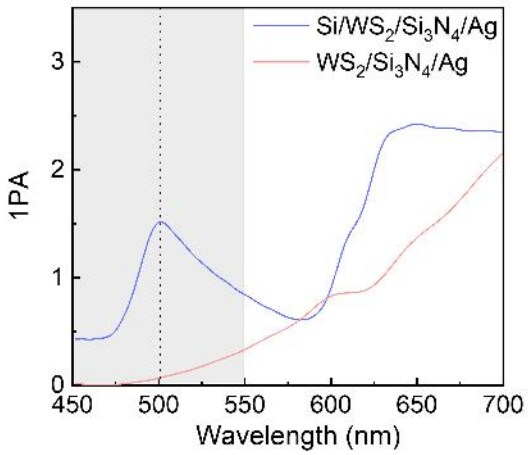

Figure S2. 1PA spectra calculated for a WS_2 monolayer on a Si_3N_4/Ag heterostructure (pink curve) and a WS_2 monolayer embedded in a Si/Si_3N_4/Ag nanocavity (d = 149.6 nm) (blue curve), respectively.

Supplementary Note 3

The in-plane electric field enhancement at emission wavelength (615 nm) determines the enhancement factor of the emission rate. In Figure S3a,b, we present the in-plane electric field distribution ($|E_{xy}|/|E_0|$) within a WS_2 monolayer in the XY plane and the electric field distribution ($|E|/|E_0|$) in the XZ plane, calculated for a Si/WS_2/Si_3N_4/Ag nanocavity (d = 149.6 nm) at its MD resonance (615 nm). For comparison, Figure S3b,c also show the corresponding electric field distributions for a larger nanocavity (d = 204.2 nm) at its ED resonance (615 nm). The in-plane electric field induced by the MD resonance is stronger and more localized compared to that induced by the ED resonance. In addition, as shown Figure S3a,c, the size of the hot spots is approximately equal to the diameter of the nanocavity.

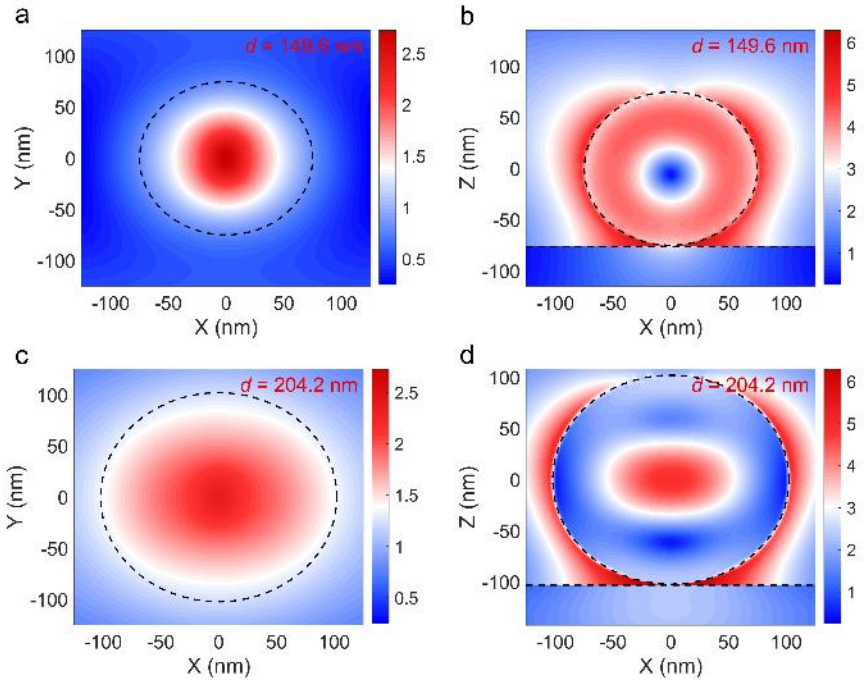

Figure S3. In-plane electric field distribution ($|E_{xy}|/|E_0|$) within a WS_2 monolayer in the XY plane (a) and electric field distribution ($|E|/|E_0|$) in the XZ plane (b), calculated for a Si/WS_2/Si_3N_4/Ag nanocavity (d = 149.6 nm) at its MD resonance (615 nm). In-plane electric field distribution ($|E_{xy}|/|E_0|$) within the WS_2 monolayer in the XY plane (c) and electric field distribution ($|E|/|E_0|$) in the XZ plane (d), calculated for a Si/WS_2/Si_3N_4/Ag nanocavity (d = 204.2 nm) at its ED resonance (615 nm).

Supplementary Note 4

In Figure S4, we show the two-dimensional radiation patterns of a *x*-polarized dipole source located on a Si_3N_4/Ag planar structure and embedded in Si/Si_3N_4/Ag nanocavities. The Si/Si_3N_4/Ag nanocavity significantly enhances the backward radiation intensity, which is over one order of magnitude higher than that of the Si_3N_4/Ag planar structure. Furthermore, the radiation intensity induced by the MD resonance (red curve) is stronger than that induced by the ED resonance (blue curve).

For low-Q dispersive systems, the Purcell factor (F_P) can be generalized as:[1,2]

$$F_P = \frac{3Q}{4\pi^2}\left(\frac{\lambda}{n}\right)^3 \mathrm{Re}\left(\frac{1}{\tilde{V}}\right), \quad (1)$$

where $\tilde{V}$ is the complex mode volume, λ is the emission wavelength at the resonance, n represents the refractive index of the medium in which the emitter is located, and Q is the quality factor of the mode. This expression reduces to the standard formula only in the high-Q cavity ($Q \to \infty$), where the mode volume in the formula becomes a real-valued form. In addition, we can directly calculate the Purcell factor by integrating the radiation intensity of a dipole emitter located at the nanocavity, as expressed below:

$$F_{\mathrm{p}} = \frac{\int\int I(\theta,\varphi)\sin\theta d\theta d\phi\big|_{\mathrm{cavity}}}{\int\int I(\theta,\varphi)\sin\theta d\theta d\phi\big|_{\mathrm{reference}}}, \quad (2)$$

where $I(\theta,\varphi)$ is the radiation intensity. Thus, the Purcell factor of the nanocavity (d = 149.6 nm) was derived to be ~3 (see Figure S4), which is consistent with values reported in the literature with similar structures.[3,4] For dielectric nanostructures with strong MD resonances, the Purcell factor reported in the literature are generally no higher than 10–15.[3] Although the Purcell factor of the nanocavity is relatively small, the PL *EF* of the Si/WS_2/Si_3N_4/Ag nanocavity under CW laser excitation is determined by the excitation rate, the quantum efficiency (i.e., Purcell effect), and emission directionality. Owing to the modulated emission directionality induced by the nanocavity, the radiation is strongly redirected toward the positive Z-axis, as shown in Figure S4. Using an oil-immersion objective with a numerical aperture (NA) of 1.3 (corresponding to a collection half-angle of ~60°), the detected PL *EF*

due to improved collection efficiency reaches as high as ~13, which is higher than the Purcell factor (F_P).

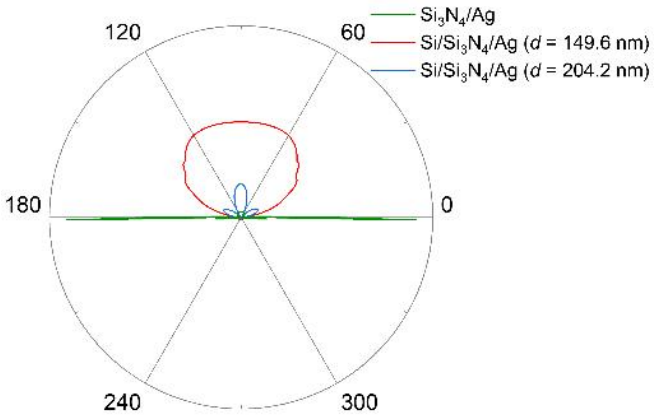

Figure S4. Two-dimensional radiation patterns in the YZ plane calculated for a Si_3N_4/Ag planar structure and two Si/Si_3N_4/Ag nanocavities (d = 149.6 nm and d = 204.2 nm), respectively, at the exciton resonant wavelength (615 nm).

Supplementary Note 5

Figure S5a presents the backward scattering spectra calculated for two different Si/WS_2/Si_3N_4/Ag nanocavities. A shallow dip is observed in each of the two scattering spectra. In Figure S5b, we show the backward scattering spectrum measured for a Si/WS_2/Si_3N_4/Ag nanocavity. One can observe a shallow dip in the scattering spectrum. In order to obtain the coupling strength (g) of the MD-exciton system, we fitted the calculated scattering spectrum based on the coupled harmonic oscillator model, as shown in Figure S5c. A coupling strength of g = 16 meV can be obtained, which does not satisfy the criterion for strong coupling ($g > (\gamma_{MD} + \gamma_{ex})/4$). Here, γ_{MD} = 170 meV and γ_{ex} = 68 meV represent the dissipation rates of the MD resonance and the exciton,[5] respectively. Thus, the interaction between the MD resonance and the exciton belongs to the weak-coupling regime. Similarly, the interaction between the ED resonance and the exciton also lies in the weak-coupling regime. Due to the limited contact area in the particle-on-film structure, the number of excitons involved in the coupling is relatively low, and these excitons are predominantly concentrated near the contact point between the nanoparticle and the film (the region of maximum electric field enhancement).[6,7] Thus, the dip observed in the scattering spectrum is not pronounced. When coupling occurs, Rabi splitting can be observed in the scattering spectrum, leading to the formation of upper and lower plexcitons. In Figure S5a, the lower plexciton exhibits a higher energy when coupled to the ED resonance than to the MD resonance. Typically, PL emission from the upper plexciton is difficult to observe, whereas only the PL emission from the lower plexciton is detected predominantly in experiments. Under fs laser excitation, the PL signal primarily arises from the WS_2 monolayer within the electron transfer region (see Figure S8), spatially adjacent to the coupling region, indicating that the enhanced PL is mainly attributed to the emission from the lower plexciton. Therefore, a distinct redshift is clearly observed in the PL spectrum (see Figure 2e), which is consistent with previous literature report.[8] In contrast, under CW laser excitation, the PL enhancement predominantly stems from the WS_2 monolayer within the hot spot. It is noteworthy that the hot spot induced by the MD resonance is smaller than that induced by the ED resonance (see Figure S3a,c). Thus, as shown in Figure 5d, most of the PL induced by the ED under the CW laser excitation originates from excitons

that are not involved in the coupling. Accordingly, it can be inferred that the PL enhancement induced by the MD resonance more accurately reflects the spectral characteristics of the lower plexciton, as shown in Figure 2d,e. Furthermore, as the MD resonance approaches the exciton resonance, the coupling strength increases, resulting in a reduction in the energy of the lower plexciton. In Figure S5d, we present the dependence of the PL peak redshift (Δw) observed for Si/WS_2/Si_3N_4/Ag nanocavities on the MD resonant wavelength under the excitation of a CW laser and a fs laser. The redshift increases as the MD resonance approaches the exciton resonance, which is also consistent with previous literature report.[8] The maximum redshifts are estimated to be ~14.2 nm and ~11.6 nm under the excitation of the CW laser and the fs laser, respectively. In addition, the more pronounced redshift observed under the CW laser excitation than to that under the fs laser excitation can likely be attributed to a combination of the higher laser power of the CW laser and the more significant thermal effects induced by the CW laser.

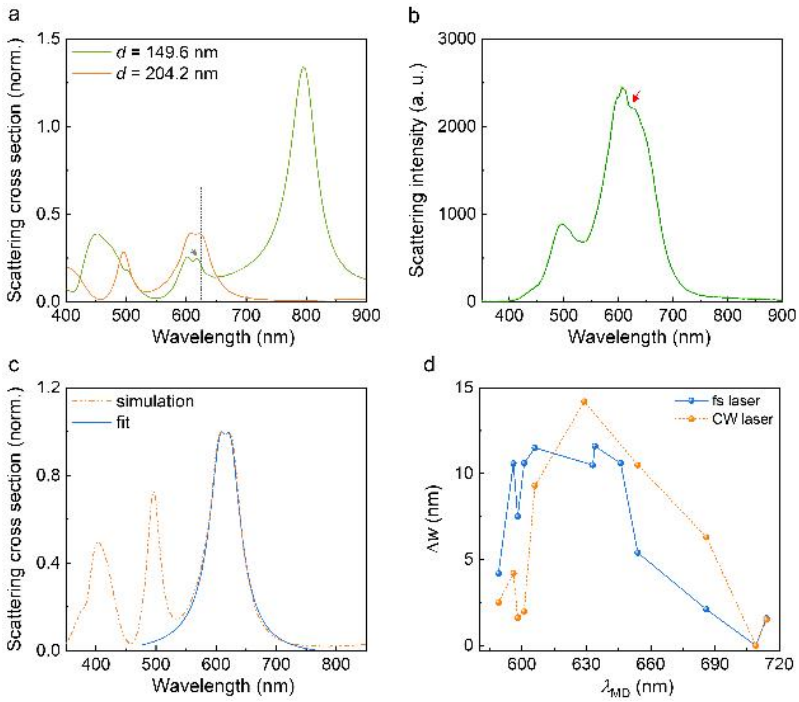

Figure S5. (a) Backward scattering spectra calculated for two Si/WS_2/Si_3N_4/Ag nanocavities (d = 149.6 nm and d = 204.2 nm). (b) Backward scattering spectrum measured for a Si/WS_2/Si_3N_4/Ag nanocavity. (c) Backward scattering spectrum calculated for a Si/WS_2/Si_3N_4/Ag nanocavity (d = 149.6 nm) (orange dashed curve) and fit result based on the coupled harmonic oscillator model (blue solid curve). (d) PL

peak redshift (Δw) observed for Si/WS_2/Si_3N_4/Ag nanocavities as a function of the MD resonant wavelength (λ_{MD}) under a CW laser (P = 60 μW) and a fs laser (P = 30 μW) excitation, respectively.

Supplementary Note 6

In Figure S6a, we present the Raman spectrum measured for a WS_2 monolayer on a Si_3N_4/Ag heterostructure. The two peaks observed at 353 and 422 cm^{-1} are attributed to the E' and A_1' modes of the WS_2 monolayer. Figure S6b presents the PL spectra of the WS_2 monolayer on Al_2O_3, Au, and Si_3N_4/Ag planar substrates, respectively. One can observe a broader linewidth of the PL spectrum for the WS_2/Si_3N_4/Ag planar structure as compared with those of the WS_2/Al_2O_3 and WS_2/Au planar structures, which is attributed to the substrate effect of the Si_3N_4/Ag heterostructure.

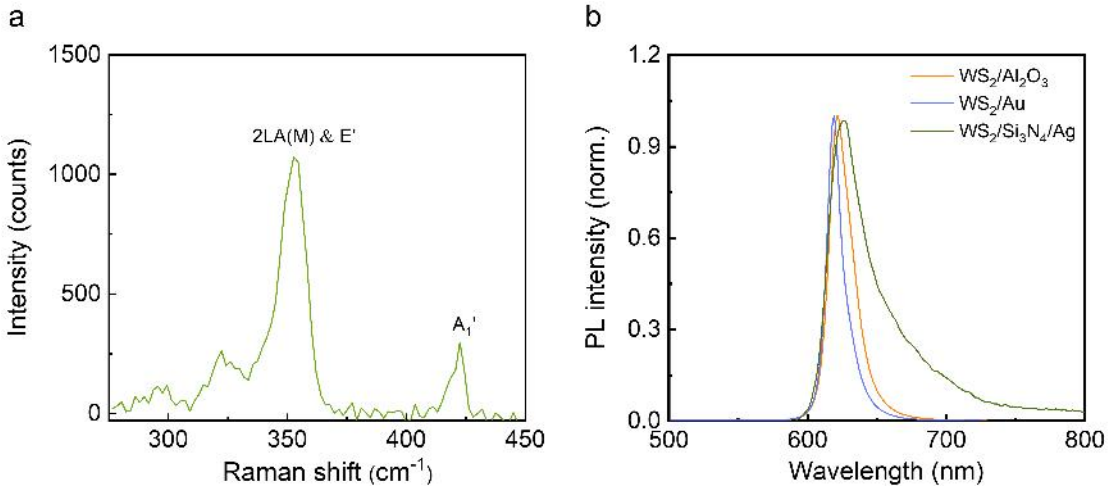

Figure S6. (a) Raman spectrum measured for a WS_2 monolayer on a Si_3N_4/Ag heterostructure. (b) PL spectra measured for a WS_2/Al_2O_3, WS_2/Au, and WS_2/Si_3N_4/Ag planar structures under the excitation of a 488-nm CW laser.

Supplementary Note 7

The laser wavelength affects the excitation efficiency of the nanocavity, which is determined by the intrinsic absorption of the materials and the electric field enhancement induced by the nanocavity resonance at the excitation wavelength. As shown in Figure 3c and Figure S9b, the PL *EF*s of nanocavities under 503 nm fs laser excitation are larger than those under 488 nm CW laser excitation. Considering that the imaginary part of the refractive index of the WS_2 monolayer (and Si) exhibits no significant difference at 488 nm and 503 nm (and 515 nm), the excitation efficiency is mainly determined by the electric field enhancement induced by the resonance. Given this experimental constraint, we adopted the alternative scheme: fixing the respective laser wavelengths (488 nm for the CW laser and 515 nm for the fs laser) while tuning the resonant wavelength of the nanocavity, as shown in Figure 2 and Figure S7. Figure S7a shows the backward scattering spectra measured for two Si/WS_2/Si_3N_4/Ag nanocavities. One can observe that the ED resonances are resonant with 488 nm but detuned from 515 nm. In Figure S7b, we present the PL spectra measured for these two Si/WS_2/Si_3N_4/Ag nanocavities and adjacent WS_2/Si_3N_4/Ag planar structures under the excitation of a 488 nm CW laser. It can be observed that the PL intensity is enhanced in both nanocavities. In addition, Figure S7c presents the PL spectra measured for these two Si/WS_2/Si_3N_4/Ag nanocavities and the adjacent WS_2/Si_3N_4/Ag planar structures under the excitation of a 515 nm fs laser. The PL intensities of the two nanocavities are significantly enhanced. It is evident that the PL enhancements of the two nanocavities excited by the fs laser are larger than those excited by the CW laser. Therefore, the significant PL enhancement observed in nanocavities is primarily attributed to the fs laser excitation, rather than the resonant excitation of the laser.

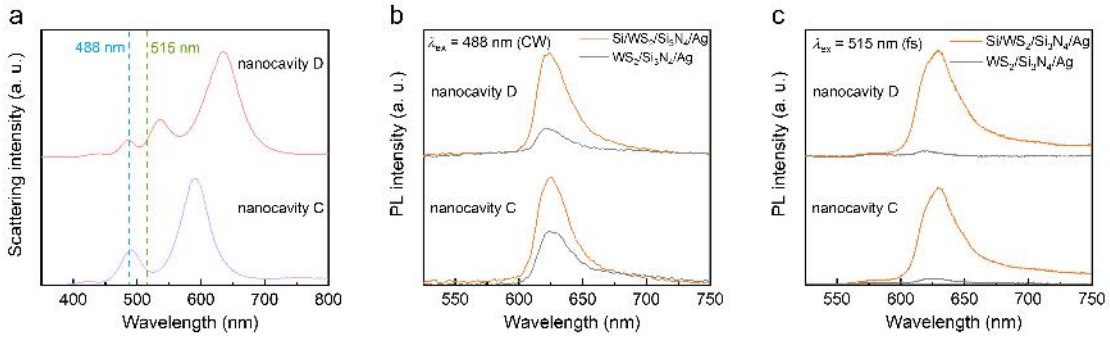

Figure S7. (a) Backward scattering spectra measured for two Si/WS_2/Si_3N_4/Ag nanocavities. (b) PL spectra measured for these two Si/WS_2/Si_3N_4/Ag nanocavities (orange curves) under the excitation of a 488 nm CW laser. PL spectra of WS_2/Si_3N_4/Ag planar structures (gray curves) are also provided for comparison. (c) PL spectra measured for these two Si/WS_2/Si_3N_4/Ag nanocavities (orange curves) under the excitation of a 515 nm fs laser. The PL spectra of the WS_2/Si_3N_4/Ag planar structures (gray curves) are also provided for comparison.

Supplementary Note 8

The PL enhancement in nanocavities mainly originates from the region (S_1) of electron transfer from a Si nanoparticle to a WS_2 monolayer. As shown in Figure S8a, the diameter of the charge transfer region is markedly smaller than that of the laser spot (~1.0 μm), implying that the actual PL *EF* is substantially higher than that observed in the experiment. Basically, one can derive the PL *EF* of nanocavities under fs laser excitation by using the following formula:

$$EF = \frac{\int_{S_0} I(\mathrm{x},\mathrm{y})dS}{\int_{S_1} I(\mathrm{x},\mathrm{y})dS} \cdot \frac{I - I_0}{I_0}, \tag{3}$$

where $I(\mathrm{x},\mathrm{y})$ is the spatial intensity profile of the laser beam, S_0 is the area corresponding to the full width at half maximum of $I(\mathrm{x},\mathrm{y})$, and S_1 is the area of the charge transfer region. This region (S_1) is defined as the area within which the electric field intensity decreases from its peak value to half that maximum. In Figure S8b,c, we present the electric field distribution ($|E|/|E_0|$) and the electric field intensity distribution ($|E|^2/|E_0|^2$) within a WS_2 monolayer in the XY plane for nanocavity B. Based on this analysis, S_1 is estimated to be ~2277 nm^2. According to the formula, the PL *EF* in nanocavity B is found to be ~13729.

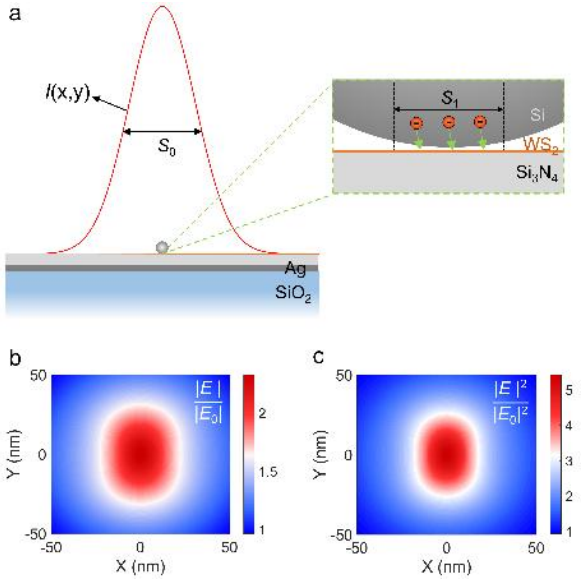

Figure S8. (a) Schematic showing the size corresponding to the full width at half maximum of *I*(x,y) (S_0) and the region of the electron transfer from a Si nanoparticle to a WS_2 monolayer (S_1). Electric field distribution ($|E|/|E_0|$) (b) and electric field intensity distribution ($|E|^2/|E_0|^2$) (c) within a WS_2 monolayer in the XY plane, calculated for nanocavity B (*d* = 153.0 nm) at its ED resonance.

Supplementary Note 9

As shown in Figure S9a, we present the dependence of the relative PL intensity on the resonant wavelength of the MD resonance (λ_{MD}) supported by Si/WS_2/Si_3N_4/Ag nanocavities. For the nanocavities excited by a 488 nm CW laser, the relative PL intensity first increases and then decreases with increasing λ_{MD}. It reaches its maximum value (~5.1) when the MD resonance is close to the exciton resonance. Additionally, under the excitation of a 515 nm fs laser, the relative PL intensity shows a similar dependence on the λ_{MD}, with a maximum value of ~54.5 occurring at 630 nm (nanocavity B). Moreover, we present the relative PL intensity of two Si/WS_2/Si_3N_4/Ag nanocavities as a function of the excitation wavelength of a fs laser, as shown in Figure S9b. For nanocavity A, we observe a rapid increase in the relative PL intensity from ~7.5 to ~17.9 as the excitation wavelength increases to 518 nm. Beyond this wavelength, it quickly decreases to ~12.1 at 536 nm. For nanocavity B, the relative PL intensity also increases sharply from ~26.7 to a maximum of ~48.3 at λ_{ex} = 513 nm, before falling to ~17.6 at λ_{ex} = 536 nm.

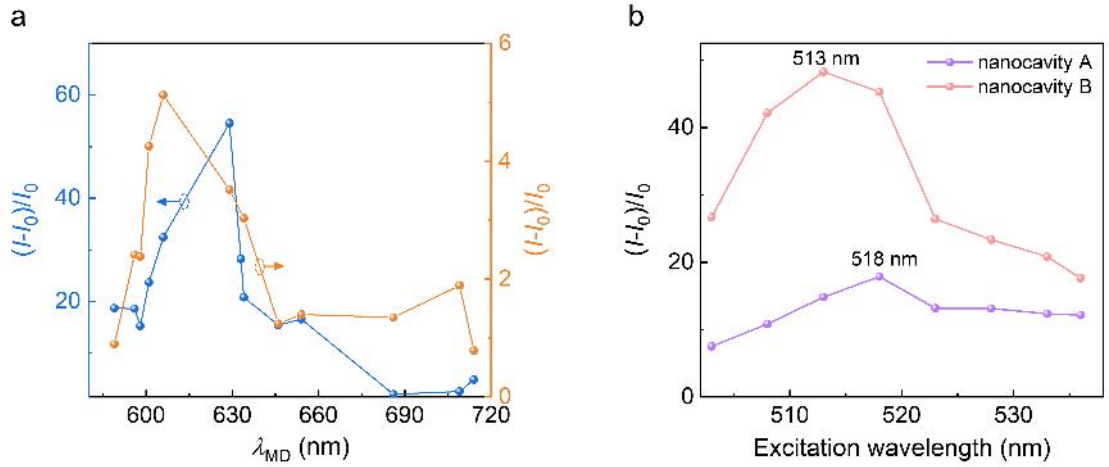

Figure S9. (a) Dependence of the relative PL intensity on the resonant wavelength of the MD resonance (λ_{MD}) supported by Si/WS_2/Si_3N_4/Ag nanocavities at the excitation of a 488 nm CW laser (orange curve) and a 515 nm fs laser (blue curve), respectively. (b) Relative PL intensity of two Si/WS_2/Si_3N_4/Ag nanocavities as a function of the fs laser excitation wavelength at a laser power of P = 30 μW.

References

[1] P. Lalanne, W. Yan, K. Vynck, C. Sauvan, J. P. Hugonin, Light Interaction with Photonic and Plasmonic Resonances. *Laser Photonics Rev.* **2018**, *12*, 1700113.

[2] P. T. Kristensen, S. Hughes, Modes and Mode Volumes of Leaky Optical Cavities and Plasmonic Nanoresonators. *ACS Photonics* **2013**, *1*, 2.

[3] A. Krasnok, S. Glybovski, M. Petrov, S. Makarov, R. Savelev, P. Belov, C. Simovski, Y. Kivshar, Demonstration of the Enhanced Purcell Factor in All-Dielectric Structures. *Appl. Phys. Lett.* **2016**, *108*, 211105.

[4] D. G. Baranov, R. S. Savelev, S. V. Li, A. E. Krasnok, A. Alù, Modifying Magnetic Dipole Spontaneous Emission with Nanophotonic Structures. *Laser Photonics Rev.* **2017**, *11*, 1600268.

[5] F. Shao, S. Y. Woo, N. Wu, R. Schneider, A. J. Mayne, S. M. de Vasconcellos, A. Arora, B. J. Carey, J. A. Preuß, N. Bonnet, M. Och, C. Mattevi, K. Watanabe, T. Taniguchi, Z. Niu, R. Bratschitsch, L. H. G. Tizei, Substrate Influence on Transition Metal Dichalcogenide Monolayer Exciton Absorption Linewidth Broadening. *Phys. Rev. Mater.* **2022**, *6*, 074005.

[6] H. Wang, J. Wen, W. Wang, N. Xu, P. Liu, J. Yan, H. Chen, S. Deng, Resonance Coupling in Heterostructures Composed of Silicon Nanosphere and Monolayer WS_2: A Magnetic-Dipole-Mediated Energy Transfer Process. *ACS Nano* **2019**, *13*, 1739.

[7] S. Lepeshov, M. Wang, A. Krasnok, O. Kotov, T. Zhang, H. Liu, T. Jiang, B. Korgel, M. Terrones, Y. Zheng, A. Alu, Tunable Resonance Coupling in Single Si Nanoparticle-Monolayer WS_2 Structures. *ACS Appl. Mater. Interfaces* **2018**, *10*.

[8] Y. Jiang, H. Wang, S. Wen, H. Chen, S. Deng, Resonance Coupling in an Individual Gold Nanorod-Monolayer WS_2 Heterostructure: Photoluminescence Enhancement with Spectral Broadening. *ACS Nano* **2020**, *14*, 13841.